

Journal Pre-proofs

Oxygen vacancy-enriched $V_2O_5 \cdot nH_2O$ nanofibers ink for universal substrates-tolerant and multi means-integratable NH_3 sensing

Xi Xia Xing, Xin Hua Zhao, Zhen Xu Li, Ling Ling Du, Chen Wang, Dong Liang Feng, Dong Sheng Geng, Robert Bogdanowicz, Dach i Yang

PII: S1385-8947(23)05964-8
DOI: <https://doi.org/10.1016/j.cej.2023.147233>
Reference: CEJ 147233

To appear in: *Chemical Engineering Journal*

Received Date: 16 July 2023
Revised Date: 22 September 2023
Accepted Date: 7 November 2023

Please cite this article as: X. Xing, X. Zhao, Z. Li, L. Du, C. Wang, D. Feng, D. Geng, R. Bogdanowicz, D. Yang, Oxygen vacancy-enriched $V_2O_5 \cdot nH_2O$ nanofibers ink for universal substrates-tolerant and multi means-integratable NH_3 sensing, *Chemical Engineering Journal* (2023), doi: <https://doi.org/10.1016/j.cej.2023.147233>

This is a PDF file of an article that has undergone enhancements after acceptance, such as the addition of a cover page and metadata, and formatting for readability, but it is not yet the definitive version of record. This version will undergo additional copyediting, typesetting and review before it is published in its final form, but we are providing this version to give early visibility of the article. Please note that, during the production process, errors may be discovered which could affect the content, and all legal disclaimers that apply to the journal pertain.

© 2023 Elsevier B.V. All rights reserved.



1 Oxygen Vacancy-enriched $V_2O_5 \cdot nH_2O$ Nanofibers Ink for Universal 2 Substrates-tolerant and Multi Means-integratable NH_3 Sensing

3 Xiaxia Xing ^a, Xinhua Zhao ^a, Zhenxu Li ^a, Lingling Du ^a, Chen Wang ^a, Dongliang Feng ^a,
4 Dongsheng Geng ^b, Robert Bogdanowicz ^c, Dachi Yang ^{a,*}

5

6 ^a Tianjin Key Laboratory of Optoelectronic Sensor and Sensing Network Technology,
7 Engineering Research Center of Thin Film Optoelectronics Technology, Ministry of
8 Education and Department of Electronics, College of Electronic Information and Optical
9 Engineering, Nankai University, Tianjin 300350, P. R. China

10 E-mail: yangdachi@nankai.edu.cn

11 ^b School of Materials Science and Engineering, University of Science and Technology
12 Beijing, Beijing, 100083, P. R. China

13 ^c Department of Metrology and Optoelectronics, Faculty of Electronics,
14 Telecommunications and Informatics, Gdansk University of Technology, 11/12G.
15 Narutowicza St., 80-233 Gdansk, Poland

16

17 **Abstract** : Universal substrates-tolerant and multi means-integratable ammonia (NH_3)
18 sensing is highly desired in future Internet of Things in environmental monitoring, food security
19 and early diagnosis of human diseases, however, is still less than satisfactory. Here, an oxygen
20 vacancy-governed NH_3 sensing has been developed with $V_2O_5 \cdot nH_2O$ nanofibers (NFs) ink, via
21 combined thermal decomposition of ammonium metavanadate and dilution. As-obtained NH_3
22 sensing ink takes on red colloids, in which the $V_2O_5 \cdot nH_2O$ NFs around 14 nm in diameter are
23 interconnected. Beneficially, the fabric fiber decorated with $V_2O_5 \cdot nH_2O$ NFs ink displays
24 excellent selectivity and ppb-concentration detection limit. Remarkably, $V_2O_5 \cdot nH_2O$ NFs ink
25 is integrated over “hard” and “flexible” substrates such as glass, wood, paper, leaf and fabric
26 with excellent tolerance by multi-integratable means such as writing, dipping and sewing.
27 Theoretically, such NH_3 sensing is interpreted that the bonding between V_2O_5 NFs and H_2O
28 modulates oxygen vacancy and thus adsorption sites, and the incorporation between crystal
29 water and free one contributes to stable ink. Practically, A sensing device built with
30 $V_2O_5 \cdot 3.1H_2O$ NFs ink has been simulated to communicate with a smartphone with reliable NH_3
31 sensing.

32 **Keywords:** Oxygen vacancy; $V_2O_5 \cdot nH_2O$ nanofibers sensing ink; Universal substrates-
33 tolerant; Multi means-integratable; Ammonia sensing

34

35 1. Introduction

36 Ammonia (NH_3), as a promising energy carrier [1, 2], may damage human organs if the long-
37 term exposure to NH_3 is larger than 25 ppm due to its corrosive and toxic nature [3, 4]. Instead,
38 NH_3 may serve as a tracer of food spoilage [5] and an exhaled biomarker of impaired kidney
39 [6] and liver function. As such, NH_3 sensing is potentially utilized in intelligent environmental
40 monitoring, food security and early diagnosis of human diseases, which is simultaneously
41 required with excellent selectivity and stability, and ppb-level detection limit. Generally, a
42 universal substrates-tolerant and multi means-integratable NH_3 sensing may contribute to
43 intelligent monitoring in the upcoming Internet of Things, although great progress has been
44 made, it needs further exploring.

45 Actually, an NH_3 sensing material with modulated sensing performance plays a crucial
46 role in the compatible integration over universal substrates by available means. As the NH_3
47 sensing materials, semiconducting metal oxides (SMOs) have been widely investigated [7-9],
48 however, their challenging issues may limit their future applications. Firstly, oxygen vacancy
49 may contribute to gas sensing of SMOs materials. Theoretically, the reaction between reducing
50 gas such as NH_3 and ionized oxygen species would be boosted due to the enhanced adsorption
51 of O_2 on oxygen vacancy [10, 11]. Accordingly, the means that can generate more oxygen
52 vacancies such as H_2 plasma treatment [12], doping [13] and annealing [10, 11] have been
53 utilized to improve the sensing performance, however, the strategies needs further developing.
54 Secondly, the nano/micro-structured NH_3 sensing SMOs are usually endowed with powder
55 form, and their suspension in an aqueous solution may agglomerate and peel off the utilized
56 substrate [14, 15]. Even being temporarily integrated, further mechanical manipulation may
57 also cause similar peeling off [16]. Thirdly, the tolerance of the sensing materials to universal
58 substrates by facially integrating means is still less than satisfactory. Conductive polymers
59 (CPs) as NH_3 sensing materials have been integrated over “hard” substrates such as glass [17]
60 and ceramic [18] and “flexible” substrates such as polyethylene terephthalate (PET) [19] and
61 paper [20]. Nevertheless, the substrates are still limited and their available integratable means
62 require either complicated procedures or proficient technicians [6, 19]. Ideally, a NH_3 sensing
63 material is tolerant to various substrates by multi-integratable means and its sensing
64 performance can be improved by an ingenious strategy, however, little has been reported so far.

65 V_2O_5 as a transition metal oxide presents unique electrical and sensing performance [21],
66 in which vanadium ions (V^{5+}) with an oxidation state generate the active sites for adsorbing
67 gaseous molecules and catalyze reactions [22]. Compared with crystalline V_2O_5 , $\text{V}_2\text{O}_5 \cdot n\text{H}_2\text{O}$
68 has been investigated with a low crystallization, which is subjected to less mechanical stress
69 and thus offers more active sites than their crystalline counterparts during reaction [23]. Notably,
70 the presence of crystal water has been reported to boost the electrochemical reaction kinetics
71 [24]. Being inspired, an oxygen vacancy-enriched $\text{V}_2\text{O}_5 \cdot n\text{H}_2\text{O}$ nanofibers (NFs) ink with a sol
72 form in this study has been developed for universal substrates-tolerant and multi means-
73 integratable NH_3 sensing at room temperature. As characterized, the $\text{V}_2\text{O}_5 \cdot n\text{H}_2\text{O}$ NFs of ~ 14
74 nm in diameter are interconnected to form red and highly dispersed ink with a zeta potential of
75 ~ 38.8 mV. Beneficially, the response of diluted $\text{V}_2\text{O}_5 \cdot 3.1\text{H}_2\text{O}$ NFs fabric to 10 ppm NH_3 have
76 been improved ($S = 17.8\%$) compared with that of pristine one ($S = 8.6\%$). Furthermore, the
77 diluted $\text{V}_2\text{O}_5 \cdot 3.1\text{H}_2\text{O}$ NFs fabric fiber shows 100 ppb detection limit of NH_3 and excellent
78 selectivity. Remarkably, the $\text{V}_2\text{O}_5 \cdot n\text{H}_2\text{O}$ NFs ink has been integrated on various substrates such
79 as ceramics, glass, wood, paper, fabric and leaf, by which multi-integratable means of writing,
80 dipping and sewing have been applied. Such sensing ink would contribute to the diversification
81 of NH_3 sensors in future intelligent sensing.

82

83 2. Experimental section

84 2.1 Synthesis of $V_2O_5 \cdot 2.3H_2O$ NFs ink [25]

85 Firstly, 1 g ammonium metavanadate (NH_4VO_3) was ground with deionized (D.I.) water, and
86 then the fluid was mixed with 10 mL of 1M HCl under continuous stirring. Secondly, when the
87 suspension turns red, D.I. water was added to make the total volume of 20 mL, the supernatant
88 was removed after precipitation. Thirdly, the red precipitate was dispersed into 80-90 °C hot
89 water to a total volume of 20 mL, the supernatant was removed after stirring and precipitating.
90 Finally, the dark red $V_2O_5 \cdot 2.3H_2O$ NFs dispersions were filled with 80-90 °C hot water to a
91 total volume of 40 mL for the subsequent utilization.

92 2.2 Synthesis of sensing fabrics and fabrics fiber integrating $V_2O_5 \cdot nH_2O$ NFs ink

93 Synthesis of $V_2O_5 \cdot nH_2O$ NFs fabrics is briefly described as follows. Initially, 0.5 mL, 2 mL
94 and 5 mL of the above synthesized $V_2O_5 \cdot 2.3H_2O$ NFs ink were ultrasonically dispersed in 10
95 mL D.I. water, respectively. Correspondingly, they are denoted as ink-0.5, ink-2 and ink-5 in
96 Fig. 3a, respectively. Secondly, the rectangular polyester fabric (2 cm×0.5 cm) and fabric fiber
97 (Diameter: ~ 207 μm, Length: ~ 2 cm) was immersed in the above synthesized $V_2O_5 \cdot nH_2O$ NFs
98 dispersion for 1 min. Finally, the $V_2O_5 \cdot nH_2O$ NFs fabrics and fabric fiber were dried at room
99 temperature. In the same way, the sensing ink was integrated over the PET and paper in Fig. 5e.
100 It should be noted that 2 mL of the pristine $V_2O_5 \cdot 2.3H_2O$ NFs ultrasonically dispersed in 10
101 mL D.I. water was defined as diluted $V_2O_5 \cdot 3.1H_2O$ NFs ink, which was taken as an example
102 for deep investigation.

103 2.3 Synthesis of $V_2O_5 \cdot 2.3H_2O$ NFs aerogel and powder, and V_2O_5 NFs powder

104 The $V_2O_5 \cdot 2.3H_2O$ NFs ink was firstly frozen at -18 °C and then lyophilized at -51 °C in a
105 freeze-drier (FD-1A-50, Henan Brothers Instrument and Equipment Co., Ltd., China) to obtain
106 $V_2O_5 \cdot 2.3H_2O$ NFs aerogel. The $V_2O_5 \cdot 2.3H_2O$ NFs aerogel was grounded using an agate mortar
107 to obtain $V_2O_5 \cdot 2.3H_2O$ NFs powder, its resistivity was tested under various pressures (2-30
108 MPa) in Fig. S1, in which the resistivity mean is ~ 7823 Ωcm. The $V_2O_5 \cdot 2.3H_2O$ NFs powder
109 was annealed in air at 600 °C for 2 h to remove the crystal water, then the V_2O_5 NFs powder
110 was collected.

111 2.4 Characterization

112 The samples were characterized by field emission scanning electron microscopy (FE-SEM,
113 JSM-7800) with energy dispersive X-ray spectroscopy (EDS, Oxford), transmission electron
114 microscopy (TEM, JEM-2200FS), X-ray diffraction (XRD, Rigaku Smart Lab 3kW) using Cu
115 $K\alpha$ radiation, Raman spectra (SR-500I-A, a wavelength of 532 nm as the excitation),
116 Ultraviolet-visible diffuse reflectance spectra (Shimadzu UV-3600), Mott-Schottky test
117 (electrochemistry workstation VersaSTAT 4, AMETEK Princeton), thermogravimetric
118 analysis (TGA) (Netzsch STA449F5 instrument, temperature range 30-600 °C, heating rate
119 10 °C/min, in nitrogen atmosphere), Automatic powder resistivity tester (ST2742B), Zeta
120 potential analyzer (Malvern Zetasizer Nano ZS ZEN3600, UK), electron paramagnetic
121 resonance (EPR) spectroscopy (Bruker EMXPLUS) and X-ray photoelectron spectroscopy
122 (XPS, Thermo Scientific ESCALAB 250Xi). The XPS spectra on binding energies of various
123 elements have been calibrated with C 1s at 284.8 eV.

124 2.5 Gas sensing measurement

125 The gas sensing was tested at room temperature (RT, ~ 25 °C) in air atmosphere. In detail, the
 126 two ends of fabric were connected to the Data Acquisition System (KEITHLEY 2701) by two
 127 gold clamps, which were placed in a homemade test chamber of 18 L with two air fans and a
 128 vaporizer. Notably, the NH₃ sensing is *in-situ* detection directly without other electrodes.
 129 Additionally, the gaseous and dry NH₃ with high-purity was adopted. The calculation of NH₃
 130 concentration is conducted by the gas distribution formula (equation 1), in which C (ppm) and
 131 φ represent the target gas concentration and volume fraction, respectively, and V₁ (mL) and V₂
 132 (mL) are denoted as the volume of target gas and testing chamber (V₂ = 18 L). The sensing
 133 response is expressed by $S = (R_g/R_a - 1) * 100\%$, of which R_a and R_g are the resistances in the air
 134 and target gas, respectively. The response/recovery time is defined as the time taken by the
 135 sensor to reach 90% of the final steady-state resistance after injecting or switching off the target
 136 gas.

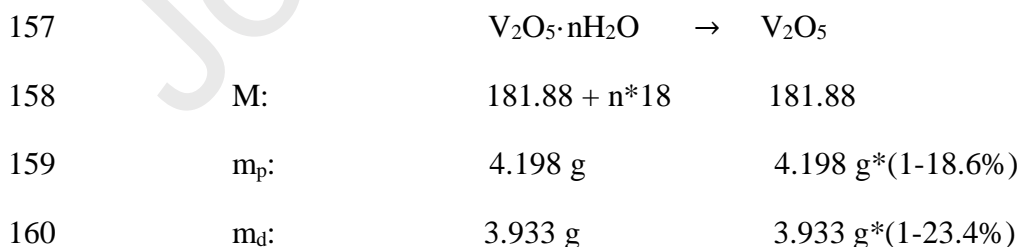
$$137 \quad V_1 = \frac{V_2 \times C}{\varphi} \times 10^{-6} \quad (1)$$

138

139 3. Results and Discussion

140 3.1. Synthesis and characterization

141 In Fig. 1a, the pristine V₂O₅·nH₂O NFs ink was diluted and integrated over fabrics, and the
 142 synthetic details of pristine V₂O₅·nH₂O NFs ink were provided in above experimental section.
 143 Meanwhile, the three-dimensional (3D) crystal structure of V₂O₅·nH₂O NFs was simulated by
 144 Visualization for Electronic and STructural Analysis (VESTA) [26]. Also, the X-ray
 145 diffractions (XRD) of pristine and diluted V₂O₅·nH₂O NFs were conducted (Fig. S2a) with the
 146 diffractive peak of V₂O₅·nH₂O at ~ 10° [27]. Meanwhile, the crystal water was removed by
 147 annealing the pristine V₂O₅·nH₂O NFs, and was then confirmed as the V₂O₅ (PDF#89-0612) in
 148 Fig. S2b. Further, Raman spectra of pristine V₂O₅·nH₂O NFs (Fig. S2c) show the V-O Raman
 149 scattering peaks with the orthorhombic crystalline [28]. Remarkably, the thermogravimetric
 150 analysis (TGA) was carried out to determine the “n” value in V₂O₅·nH₂O NFs. In Fig. 1b,
 151 weight loss of 23.4% and 18.6% occur at 100 - 600 °C, which is attributed to the loss of crystal
 152 water, and the “n” values corresponding to diluted and pristine V₂O₅·nH₂O NFs are 3.1 and 2.3,
 153 respectively. Specifically, the detailed calculation of “n” value in V₂O₅·nH₂O is described as
 154 follows. M, m_p and m_d represent relative molecular mass, mass of pristine V₂O₅·nH₂O NFs and
 155 mass of diluted one, respectively. Therefore, the “n” values corresponding to the diluted and
 156 pristine ones are calculated by the bellow proportional formula of the chemical equation.



161 In Fig. 1c, V₂O₅·3.1H₂O NFs ink is observed dense and overlapped in a lower
 162 magnification with scanning electron microscopy (SEM). While in a closer observation under
 163 transmission electron microscopy (TEM), the diameter of V₂O₅·nH₂O NFs in Fig. 1d is
 164 measured ~ 14 nm (Fig. S3). Moreover, the high-resolution TEM (HR-TEM) image and
 165 selected area electron diffraction (SAED) pattern in Fig. 1f and Fig. S4 show the (102) plane of

166 V_2O_5 (PDF#89-0612). Further, the elemental mappings under TEM (Fig. S5) verified the
 167 existence of V and O elements, and the diameter of the fabric fiber integrated with diluted
 168 $V_2O_5 \cdot 3.1H_2O$ NFs ink was measured $\sim 207 \mu m$ in Fig. 1g₁. By comparing with the shape of
 169 pristine fabric fiber in Fig. 1h₁, the flake shape in Fig. 1g₂ reveals that the $V_2O_5 \cdot 3.1H_2O$ NFs
 170 ink has been integrated over fabrics. Interestingly, the Tyndall effects of pristine and various
 171 diluted ink were compared in Fig. S6, the dispersibility of pristine $V_2O_5 \cdot 2.3H_2O$ NFs ink can
 172 be improved via dilution.

173 3.2. The stable $V_2O_5 \cdot nH_2O$ NFs ink for dilution-modulated NH_3 sensing

174 To get insight into the role of water in $V_2O_5 \cdot nH_2O$ NFs ink, the free water was initially removed
 175 by freezing and drying $V_2O_5 \cdot 2.3H_2O$ NFs ink, and then the lyophilized ones were annealed to
 176 remove crystal water and obtain V_2O_5 for subsequent comparison. In Fig. S7, the color of
 177 $V_2O_5 \cdot 2.3H_2O$ NFs powder changed from its pristine dark red to orange after annealing. The
 178 V_2O_5 and $V_2O_5 \cdot 2.3H_2O$ NFs powder were ultrasonically dispersed into D.I. water and pure
 179 ethanol, respectively. Correspondingly, various dispersions were dripped over interdigital
 180 electrodes in Fig. 2d for comparing their NH_3 sensing performance, and the real-time resistance
 181 curves were shown in Fig. 2a.

182 In Fig. 2b-c, the $V_2O_5 \cdot 2.3H_2O$ NFs exhibit a higher response to 10 ppm NH_3 than that of
 183 V_2O_5 NFs in both water and pure ethanol solvent, revealing the crystal water-boosted NH_3
 184 sensing. Actually, water solvent may contribute to lower baseline resistance in both V_2O_5 and
 185 $V_2O_5 \cdot nH_2O$ NFs (Fig. 2c). Further, free water is required in preparing $V_2O_5 \cdot nH_2O$ NFs ink in
 186 Fig. 2e. Otherwise, uneven and unstable dispersion can be obtained. Meanwhile, the
 187 $V_2O_5 \cdot 2.3H_2O$ NFs ink and ethanol dispersion were dipped over fabric in Fig. 2d₁. In Fig. S8,
 188 the resistance value of $V_2O_5 \cdot 2.3H_2O$ NFs ink fabric is $\sim 0.49 M\Omega$, however, the one with
 189 ethanol dispersion is larger than $20 M\Omega$, which reveals that the uniform and stable $V_2O_5 \cdot 2.3H_2O$
 190 NFs ink contribute to integrating conductive fabric. Notably, if one deliberately removed the
 191 crystal water in $V_2O_5 \cdot 2.3H_2O$ NFs or replaced the dispersion medium from water to pure
 192 ethanol, the dispersed phase is obviously separated from dispersion medium (Fig. 2e), rather
 193 than obtaining stable ink. As such, the incorporation of crystal water bonded by V_2O_5 with free
 194 water in the dispersion medium plays a pivotal role in the formation of sensing ink.

195 The diluted $V_2O_5 \cdot 3.1H_2O$ and pristine $V_2O_5 \cdot 2.3H_2O$ NFs inks were observed with the
 196 variation of Tyndall effect in Fig. 2f and g, in which the light path penetrates after diluting with
 197 high dispersibility of colloid [29]. Meanwhile, the simulated 3D crystalline structures with
 198 various oxygen vacancies of diluted and pristine $V_2O_5 \cdot nH_2O$ NFs are shown in Fig. 2f₁ and g₁,
 199 respectively. With the pristine $V_2O_5 \cdot 2.3H_2O$ NFs ink for comparisons, the diluted $V_2O_5 \cdot 3.1H_2O$
 200 NFs ink was integrated over the fabric (2 cm \times 0.5 cm) and the fabric fiber (Diameter: $\sim 207 \mu m$,
 201 Length: ~ 2 cm), respectively. In the photographs of Fig. 2f and g, the color of diluted
 202 $V_2O_5 \cdot 3.1H_2O$ NFs fabrics was seen lighter than that of pristine $V_2O_5 \cdot 2.3H_2O$ ones. To further
 203 gain insight into the role of dilution, the NH_3 sensing performance of the above integrated
 204 various pristine $V_2O_5 \cdot 2.3H_2O$ and diluted $V_2O_5 \cdot 3.1H_2O$ NFs fabric were investigated with
 205 comparison. In Fig. 2h, the recovery speed of pristine $V_2O_5 \cdot 2.3H_2O$ NFs fabric is improved by
 206 both diluting and adopting the fabric fiber. Meanwhile, the responses toward 5 ppm and 25 ppm
 207 NH_3 were summarized in Fig. 2i, and show that the sensing responses of diluted $V_2O_5 \cdot 3.1H_2O$
 208 NFs ink onto both fabric and fabric fiber are higher than those of pristine ones. Moreover, the
 209 real-time responses to 1-50 ppm NH_3 were evaluated in Fig. 2j, which further reveals the
 210 dilution improved NH_3 sensing performance.

211 3.3. Evaluation of the NH_3 sensing performance

212 The content of $V_2O_5 \cdot nH_2O$ NFs in the sensing ink governs the NH_3 sensing. In Fig. 3a, the
 213 responses of pristine and various diluted $V_2O_5 \cdot nH_2O$ NFs fabric to 10 ppm NH_3 were evaluated,
 214 and the $V_2O_5 \cdot nH_2O$ -2 mL NFs fabric manifested the highest response ($S = 17.8\%$) compared
 215 with pristine ones ($S = 8.6\%$), and was thus chosen for subsequent evaluation and renamed by
 216 $V_2O_5 \cdot 3.1H_2O$ NFs fabric. The response and recovery time were evaluated to ~ 75 s and 36 s
 217 toward 1 ppm NH_3 in Fig. S9, respectively. Remarkably, the flexibility of $V_2O_5 \cdot nH_2O$ NFs
 218 fabric was investigated by testing their responses to 1 ppm and 10 ppm NH_3 upon the bending
 219 angle at 0° , 45° , 90° and 360° , respectively. Excitedly, little difference was observed in Fig. 3b,
 220 indicating excellent flexibility.

221 The stability and selectivity are crucial parameters for NH_3 sensing. Remarkably, the
 222 sensing evaluation to 5 ppm NH_3 is repeated for 126 days' durations in Fig. 3c with good
 223 stability. Furthermore, the responses of various interfering gases and 10 ppm target NH_3 were
 224 compared in Fig. 3d, revealing excellent selectivity. Meanwhile, the NH_3 sensing of three
 225 $V_2O_5 \cdot 2.3H_2O$ NFs fabrics in Fig. S10 is compared, which shows a slight variation in response
 226 to the same concentration NH_3 and takes a good consistency. Additionally, the diluted
 227 $V_2O_5 \cdot 3.1H_2O$ NFs ink was integrated over the fabric fiber in Fig. 3e, and its low detection limit
 228 is around 100 ppb NH_3 . Towards a low NH_3 concentration (e.g., 100 ppb-1 ppm), the responses
 229 show an excellent linear relationship in Fig. 3f. While towards a high one (e.g., 1-50 ppm),
 230 excellent repeatability is observed in Fig. 3g. As a result, the $V_2O_5 \cdot nH_2O$ NFs fabric
 231 simultaneously present ppb-level detection, high selectivity and stability, excellent flexibility
 232 and low working temperature. Compared with other SMOs NH_3 sensing materials in Table 1,
 233 a gel-stated and stable ink of $V_2O_5 \cdot nH_2O$ NFs is prepared, which can be integrated over various
 234 "hard" and "flexible" substrates by multi-integratable means.

235 In our experiments, both temperature and humidity can influence the NH_3 sensing. In Fig.
 236 S11, the temperature-dependent sensing responses were observed to 20 ppm NH_3 at ~ 26 -140
 237 $^\circ C$, and the highest one takes place at room temperature (~ 26 $^\circ C$). Meanwhile, the baseline
 238 resistance and the sensing response of $V_2O_5 \cdot 3.1H_2O$ NFs fabric toward 5 ppm NH_3 decrease
 239 with humidity (Fig. S12), similar to previous SMOs [30] and to other humidity sensors [31].
 240 Such a decrease in the sensing response might be interpreted that H_2O molecules occupy
 241 adsorption sites, which weakens the reaction between NH_3 and adsorbed oxygen onto the
 242 surface of $V_2O_5 \cdot 3.1H_2O$ NFs [32], as may be addressed by covering filter membrane [33].

243 3.4. The oxygen vacancy governed NH_3 sensing mechanism

244 We experimentally investigated the chemisorbed oxygen to understand the dilution-boosted
 245 NH_3 sensing mechanism, and three characterizations on oxygen vacancy (V_o) of diluted
 246 $V_2O_5 \cdot 3.1H_2O$ NFs were performed with pristine $V_2O_5 \cdot 2.3H_2O$ ones as comparison. Firstly, the
 247 O 1s X-ray photoelectron spectroscopy (XPS) in Fig. 4a spectra were deconvoluted into three
 248 oxygen species of O_I , O_{II} and O_{III} , which are associated with oxygen atoms bound to metals,
 249 defect sites with low oxygen coordination and hydroxy species, respectively. Remarkably, the
 250 integral-area ratios of O_{II} increase from 20% of pristine $V_2O_5 \cdot 2.3H_2O$ NFs to 52% of diluted
 251 $V_2O_5 \cdot 3.1H_2O$ ones, indicating that the diluted $V_2O_5 \cdot 3.1H_2O$ one possesses more oxygen
 252 vacancies [34]. Meanwhile, the V 2p spectra in Fig. 4b correspond to the characteristics of V^{5+} ,
 253 the discrepancy in binding energy (0.3 eV) indicates distinct electronic environments of V ions
 254 in the pristine and diluted $V_2O_5 \cdot nH_2O$ NFs, which might be interpreted as increased oxygen
 255 vacancy in the diluted $V_2O_5 \cdot 3.1H_2O$ ones [10]. Secondly, the presence of oxygen vacancy was
 256 further studied by electron paramagnetic resonance (EPR) spectroscopic measurements in Fig.
 257 4c and symmetrical EPR signals ($g = 1.9612$) are assigned to the unpaired electrons in the
 258 oxygen vacancy sites [10, 35]. The ESR intensity of diluted $V_2O_5 \cdot 3.1H_2O$ NFs is higher than

259 that of pristine $V_2O_5 \cdot 2.3H_2O$ ones, indicating dilution governed the oxygen vacancy, which
 260 result in more chemisorbed oxygen for gas sensing. Thirdly, such result is also evidenced by
 261 the narrower optical bandgaps (E_g) of diluted $V_2O_5 \cdot 3.1H_2O$ NFs (1.87 eV) than that of pristine
 262 $V_2O_5 \cdot 2.3H_2O$ (2.19 eV) in Fig. 4d.

263 The energy-band variation of $V_2O_5 \cdot nH_2O$ NFs was investigated for understanding the NH_3
 264 sensing mechanism. Specifically, the valence band maximum (E_v) of the $V_2O_5 \cdot 3.1H_2O$ NFs is
 265 determined to ~ 2.4 eV (Fig. S14). Accordingly, the conduction band minimum (E_c) of
 266 $V_2O_5 \cdot 3.1H_2O$ is calculated to ~ 0.53 eV according to Equation (2). Usually, V_2O_5 is reported
 267 as a n-type semiconductor [36]. However, p-type sensing characteristic with increased
 268 resistance was observed in this study (Fig. 2a and h), which is explained as follows. The
 269 $V_2O_5 \cdot 3.1H_2O$ NFs contain abundant oxygen vacancy, which will improve chemisorption of O_2
 270 and H_2O molecule [11, 37], capture more electrons from the conduction band of $V_2O_5 \cdot nH_2O$
 271 NFs and thus bend upward band causing an inversion layer, therefore, the Fermi level (E_F)
 272 located below the intrinsic level (E_i) in Fig. 4e [38]. In the surface inversion layer, holes usually
 273 serve as the major carriers with p-type feature, which was confirmed by Mott-Schottky with a
 274 negative slope in Fig. 4e₁.

$$275 \quad E_c = E_v - E_g \quad (2)$$

276 To understand the p-type sensing mechanism, the NH_3 sensing evaluations under various
 277 working temperatures were investigated in Fig. S11, the $V_2O_5 \cdot 3.1H_2O$ NFs show increased
 278 sensing resistance to 20 ppm NH_3 at $\sim 26-80$ °C and decreased ones at $\sim 100-140$ °C. Such
 279 phenomenon is explained as follows. At lower temperatures, the strong adsorption of O_2 and
 280 H_2O molecules contribute to the formation of an inversion layer on the surface of $V_2O_5 \cdot 3.1H_2O$
 281 NFs, exhibiting p-type semiconductor properties [39]. With the elevating of temperature, an
 282 inversion layer would be destroyed without sufficient O_2 and H_2O molecules, n-type sensing
 283 behavior would be seen. Further, we conducted additional comparative experiments on NH_3
 284 sensing under insufficient oxygen conditions and air atmosphere in Fig. S15, the significantly
 285 decreased response in Fig. S15a indicates that the sufficient surface adsorption of oxygen
 286 contributes to NH_3 sensing of $V_2O_5 \cdot 3.1H_2O$ NFs.

287 Accordingly, the NH_3 sensing mechanism of $V_2O_5 \cdot nH_2O$ NFs fabrics is interpreted as
 288 follows. In Fig. 4f, when the pristine p-type $V_2O_5 \cdot 2.3H_2O$ ones are exposed to NH_3 , the pre-
 289 adsorbed oxygen species (O_2^-) and hydroxy species ($-OH$) react with NH_3 and release electrons
 290 [40, 41], reducing the hole concentration and thus elevating the resistance. Similarly, the diluted
 291 $V_2O_5 \cdot 3.1H_2O$ NFs show NH_3 sensing mechanism in Fig. 4f₁. However, the content of their
 292 oxygen vacancy is significantly increased thus improved chemisorbed oxygen, and finally
 293 present boosted NH_3 sensing.

294 **3.5. $V_2O_5 \cdot nH_2O$ NFs ink for universal substrates-tolerant and multi means-integratable** 295 **NH_3 sensing and the simulation detection of NH_3**

296 The universal-substrates tolerance and multi-means integration of $V_2O_5 \cdot 2.3H_2O$ NFs ink were
 297 investigated. The tolerance has been widely examined on hard substrates such as ceramics,
 298 stainless steel, glass and wood, and flexible ones such as Chinese “Xuan” paper, leaf, Al foil,
 299 plastic wrap and A4 size paper in Fig. 5a. Meanwhile, the adhesive performance of the
 300 $V_2O_5 \cdot 2.3H_2O$ NFs ink over the above substrate has been investigated in Fig. S16, one can see
 301 that the adhesive properties depend on the substrates and the sensing ink shows a weaker
 302 adhesion than that of commercial one on A4 paper (Fig. S17). As for the integratable means,
 303 our $V_2O_5 \cdot 2.3H_2O$ NFs ink can be dipped with a paintbrush to draw the school badge and the
 304 motto of Nankai University in Fig. 5a and other “dipping-drying” approach in Fig. 5b.

305 Impressively, the $V_2O_5 \cdot 3.1H_2O$ NFs ink can also serve as a colouring agent with color variation
306 from white of pristine fabric fiber to orange, which can be integrated over the fabric fiber (Fig.
307 5c), and can even be sewed on the clothes with the “NKU” pattern. Particularly, by freezing
308 and drying, the $V_2O_5 \cdot 3.1H_2O$ NFs ink can be transformed into lightweight aerogel, and can
309 even stand on the tip of the reed (Fig. S18). In this case, even being storing 365 days (Fig. 5d)
310 and 608 days (Fig. S19a), the $V_2O_5 \cdot 3.1H_2O$ NFs ink remains excellent dispersibility and
311 stability, which is verified by characterizing the zeta potential of $V_2O_5 \cdot 3.1H_2O$ NFs ink to ~
312 38.8 mV after storing 608 days (Fig. S19b).

313 As examples, the PET, Chinese “Xuan” paper and fabric integrated with $V_2O_5 \cdot 3.1H_2O$
314 NFs ink were examined for their NH_3 sensing performance in Fig. 5e, showing substrates-
315 dependent NH_3 sensing, which may be explained that these bare and insulated substrates serve
316 as support and don't participate electron transport. Although previous investigations (Table 1)
317 have made great progress, our $V_2O_5 \cdot nH_2O$ NFs ink is the one that can be simultaneously utilized
318 for universal substrates-tolerant and multi means-integratable NH_3 sensing. Practically, such
319 NH_3 sensing ink enable to be integrated into the feasible substrates such as smocks, mask and
320 food packaging bag for environmental monitoring, exhaled diagnosis of human diseases and
321 inspection of food safety. Herein, we elaborately integrated the $V_2O_5 \cdot 3.1H_2O$ NFs ink onto the
322 polyethylene sample bag (4 cm×6 cm) as an example, to simulate detection of NH_3 , which was
323 read by a smartphone (Fig. 5f). Specifically, the microcontroller NodeMCU (ESP8266, 5.8
324 cm×3.1 cm) with Wireless Fidelity (Wi-Fi) module communicate with the smartphone and
325 perform the NH_3 sensing and alarming of the device. In the supplemental video, when 10 ppm
326 NH_3 was injected and the sensing voltage is lower than the alarm threshold (0.5 V), the
327 smartphone read “ALARMING!” (Fig. 5g). Conversely, the NH_3 being released with the one
328 higher than 0.5 V, and “Monitoring” in smartphone is seen. Also, the detailed historical
329 information can be read and recorded in Fig. 5h, which is great potential for inspection of food
330 safety.

331

332 4. Conclusion

333 To summarize, an oxygen vacancy-enriched $V_2O_5 \cdot nH_2O$ NFs ink has been developed by
334 combining the thermal decomposition of ammonium metavanadate with subsequent dilution,
335 for universal substrates-tolerant and multi means-integratable NH_3 sensing at room temperature.
336 Experimentally, the $V_2O_5 \cdot nH_2O$ NFs of ~ 14 nm in diameter were observed to be interconnected,
337 forming red colloids in an aqueous solution with high dispersibility. Theoretically, the bonding
338 between V_2O_5 NFs and H_2O governs the oxygen vacancy with improved the adsorption sites of
339 NH_3 , and the incorporation between crystal water and free water contributes to stable ink.
340 Beneficially, the diluted $V_2O_5 \cdot 3.1H_2O$ NFs fabrics show an increased response to 10 ppm NH_3
341 ($S = 17.8\%$) compared with the pristine ones ($S = 8.6\%$). Also, the $V_2O_5 \cdot nH_2O$ NFs ink fabric
342 fiber displays excellent selectivity and ppb-level detection limit to NH_3 . Remarkably,
343 $V_2O_5 \cdot nH_2O$ NFs ink has been integrated over various substrates such as ceramics, glass, wood,
344 paper, fabric and leaf with universal substrates-tolerance. Meanwhile, multiple strategies of
345 writing, dipping and sewing have been adopted for integration. As an example of application,
346 the developed oxygen vacancy-enriched $V_2O_5 \cdot 3.1H_2O$ NFs ink has been integrated into a
347 sensing device and communicates with a smartphone with reliable monitoring and alarming,
348 which is potential in future intelligent sensing of Internet of Things. Future investigations are
349 expected to be conducted on theoretical calculations and humidity-dependent NH_3 sensing.

350

351 Declaration of Competing Interest

352 The authors declare that they have no known competing financial interests or personal
353 relationships that could have appeared to influence the work reported in this paper.

354

355 Data availability

356 Data will be made available on request.

357

358 Acknowledgements

359 This work was financially supported by the National Natural Science Foundation of China
360 (Grant No. 52072184) and Tianjin Research Innovation Project for Postgraduate Students
361 (General Project, Grant No. 2022BKY035).

362

363 References

- 364 [1] W. Gao, J. Guo, P. Wang, Q. Wang, F. Chang, Q. Pei, W. Zhang, L. Liu, P. Chen,
365 Production of ammonia via a chemical looping process based on metal imides as nitrogen
366 carriers, *Nat. Energy* 3 (2018) 1067-1075.
- 367 [2] K. Nakajima, H. Toda, K. Sakata, Y. Nishibayashi, Ruthenium-catalysed oxidative
368 conversion of ammonia into dinitrogen, *Nat. Chem.* 11 (2019) 702-709.
- 369 [3] M. Van Damme, L. Clarisse, S. Whitburn, J. Hadji-Lazaro, D. Hurtmans, C. Clerbaux,
370 P.-F. Coheur, Industrial and agricultural ammonia point sources exposed, *Nature* 564
371 (2018) 99-103.
- 372 [4] A.T. Güntner, M. Wied, N.J. Pineau, S.E. Pratsinis, Rapid and Selective NH₃ Sensing by
373 Porous CuBr, *Adv. Sci.* 7 (2020) 1903390.
- 374 [5] Z. Ma, P. Chen, W. Cheng, K. Yan, L. Pan, Y. Shi, G. Yu, Highly Sensitive, Printable
375 Nanostructured Conductive Polymer Wireless Sensor for Food Spoilage Detection, *Nano*
376 *Lett.* 18 (2018) 4570-4575.
- 377 [6] H.-Y. Li, C.-S. Lee, D.H. Kim, J.-H. Lee, Flexible Room-Temperature NH₃ Sensor for
378 Ultrasensitive, Selective, and Humidity-Independent Gas Detection, *ACS Appl. Mater.*
379 *Interfaces* 10 (2018) 27858-27867.
- 380 [7] B. Yang, X. Li, W. Yuan, Z. Li, N. Lu, S. Wang, Y. Wu, S. Fan, Z. Hua, Efficient NH₃
381 Detection Based on MOS Sensors Coupled with Catalytic Conversion, *ACS Sens.* 5
382 (2020) 1838-1848.
- 383 [8] S. Kumar, A. Singh, R. Singh, S. Singh, P. Kumar, R. Kumar, Facile h-MoO₃ synthesis
384 for NH₃ gas sensing application at moderate operating temperature, *Sens. Actuator B*
385 *Chem.* 325 (2020) 128974.



- 386 [9] Y.-Y. Li, J.-L. Chen, F.-L. Gong, G.-X. Jin, K.-F. Xie, X.-Y. Yang, Y.-H. Zhang, Dual
387 functionalized Ni substitution in shuttle-like In_2O_3 enabling high sensitivity NH_3
388 detection, *Appl. Surf. Sci.* 600 (2022) 154158.
- 389 [10] H. Yuan, S.A.A.A. Aljneibi, J. Yuan, Y. Wang, H. Liu, J. Fang, C. Tang, X. Yan, H. Cai,
390 Y. Gu, S.J. Pennycook, J. Tao, D. Zhao, ZnO Nanosheets Abundant in Oxygen Vacancies
391 Derived from Metal-Organic Frameworks for ppb-Level Gas Sensing, *Adv. Mater.* 31
392 (2019) 1807161.
- 393 [11] G. Li, H. Zhang, L. Meng, Z. Sun, Z. Chen, X. Huang, Y. Qin, Adjustment of oxygen
394 vacancy states in ZnO and its application in ppb-level NO_2 gas sensor, *Sci. Bull.* 65 (2020)
395 1650-1658.
- 396 [12] Z. Geng, X. Kong, W. Chen, H. Su, Y. Liu, F. Cai, G. Wang, J. Zeng, Oxygen Vacancies
397 in ZnO Nanosheets Enhance CO_2 Electrochemical Reduction to CO, *Angew. Chem. Int.*
398 *Ed.* 57 (2018) 6054-6059.
- 399 [13] X. Wang, T. Wang, G. Si, Y. Li, S. Zhang, X. Deng, X. Xu, Oxygen vacancy defects
400 engineering on Ce-doped $\alpha\text{-Fe}_2\text{O}_3$ gas sensor for reducing gases, *Sens. Actuator B Chem.*
401 302 (2020) 127165.
- 402 [14] J.H. Kim, J.H. Han, Y.C. Jung, Y.A. Kim, Mussel adhesive protein-coated titanium oxide
403 nanoparticles for effective NO removal from versatile substrates, *Chem. Eng. J.* 378
404 (2019) 122164.
- 405 [15] M.S. Azmina, R. Md Nor, H.A. Rafeie, N.S.A. Razak, S.F.A. Sani, Z. Osman, Enhanced
406 photocatalytic activity of ZnO nanoparticles grown on porous silica microparticles, *Appl.*
407 *Nanosci.* 7 (2017) 885-892.
- 408 [16] H.-R. Lim, H.S. Kim, R. Qazi, Y.-T. Kwon, J.-W. Jeong, W.-H. Yeo, Advanced Soft
409 Materials, Sensor Integrations, and Applications of Wearable Flexible Hybrid Electronics
410 in Healthcare, Energy, and Environment, *Adv. Mater.* 32 (2020) 1901924.
- 411 [17] C.-T. Lee, Y.-S. Wang, High-performance room temperature NH_3 gas sensors based on
412 polyaniline-reduced graphene oxide nanocomposite sensitive membrane, *J. Alloys.*
413 *Compd.* 789 (2019) 693-696.
- 414 [18] C. Liu, H. Tai, P. Zhang, Z. Ye, Y. Su, Y. Jiang, Enhanced ammonia-sensing properties
415 of PANI-TiO₂-Au ternary self-assembly nanocomposite thin film at room temperature,
416 *Sens. Actuator B Chem.* 246 (2017) 85-95.
- 417 [19] N. Tang, C. Zhou, L. Xu, Y. Jiang, H. Qu, X. Duan, A Fully Integrated Wireless Flexible
418 Ammonia Sensor Fabricated by Soft Nano-Lithography, *ACS Sens.* 4 (2019) 726-732.
- 419 [20] L. Du, D. Feng, X. Xing, C. Wang, Y. Gao, S. Sun, G. Meng, D. Yang, Nanocomposite-
420 Decorated Filter Paper as a Twistable and Water-Tolerant Sensor for Selective Detection
421 of 5 ppb–60 v/v% Ammonia, *ACS Sens.* 7 (2022) 874-883.
- 422 [21] X. Sun, R. Gao, Y. Wu, X. Zhang, X. Cheng, S. Gao, Y. Xu, L. Huo, Novel in-situ
423 deposited V_2O_5 nanorods array film sensor with enhanced gas sensing performance to n-
424 butylamine, *Chem. Eng. J.* 459 (2023) 141505.
- 425 [22] N. Panahi, M. Shirazi, M.T. Hosseinejad, Fabrication, characterization and hydrogen

- 426 gas sensing performance of nanostructured V_2O_5 thin films prepared by plasma focus
427 method, *J. Mater. Sci. Mater. El.* 29 (2018) 13345-13353.
- 428 [23] A. Moretti, S. Passerini, Bilayered Nanostructured $V_2O_5 \cdot nH_2O$ for Metal Batteries, *Adv.*
429 *Energy Mater.* 6 (2016) 1600868.
- 430 [24] Q. Sun, H. Cheng, Y. Yuan, Y. Liu, W. Nie, K. Zhao, K. Wang, W. Yao, X. Lu, J. Lu,
431 Uncovering the Fundamental Role of Interlayer Water in Charge Storage for Bilayered
432 $V_2O_5 \cdot nH_2O$ Xerogel Cathode Materials, *Adv. Energy Mater.* 13 (2023) 2202515.
- 433 [25] K. Zhou, Y. He, Q. Xu, Q.e. Zhang, A.a. Zhou, Z. Lu, L.-K. Yang, Y. Jiang, D. Ge, X.Y.
434 Liu, H. Bai, A Hydrogel of Ultrathin Pure Polyaniline Nanofibers: Oxidant-Templating
435 Preparation and Supercapacitor Application, *ACS Nano* 12 (2018) 5888-5894.
- 436 [26] K. Momma, F. Izumi, VESTA3 for three-dimensional visualization of crystal, volumetric
437 and morphology data, *J. Appl. Cryst.* 44 (2011) 1272-1276.
- 438 [27] C. Xiong, A.E. Aliev, B. Gnade, K.J. Balkus, Fabrication of Silver Vanadium Oxide and
439 V_2O_5 Nanowires for Electrochromics, *ACS Nano* 2 (2008) 293-301.
- 440 [28] H. Zhang, X. Han, R. Gan, Z. Guo, Y. Ni, L. Zhang, A facile biotemplate-assisted
441 synthesis of mesoporous V_2O_5 microtubules for high performance asymmetric
442 supercapacitors, *Appl. Surf. Sci.* 511 (2020) 145527.
- 443 [29] Z. Zhao, X. Wang, X. Jing, Y. Zhao, K. Lan, W. Zhang, L. Duan, D. Guo, C. Wang, L.
444 Peng, X. Zhang, Z. An, W. Li, Z. Nie, C. Fan, D. Zhao, General Synthesis of Ultrafine
445 Monodispersed Hybrid Nanoparticles from Highly Stable Monomicelles, *Adv. Mater.* 33
446 (2021) 2100820.
- 447 [30] F. Qu, S. Zhang, C. Huang, X. Guo, Y. Zhu, T. Thomas, H. Guo, J.P. Attfield, M. Yang,
448 Surface Functionalized Sensors for Humidity-Independent Gas Detection, *Angew. Chem.*
449 *Int. Ed.* 60 (2021) 6561-6566.
- 450 [31] P. Guo, B. Tian, J. Liang, X. Yang, G. Tang, Q. Li, Q. Liu, K. Zheng, X. Chen, W. Wu,
451 An All-Printed, Fast-Response Flexible Humidity Sensor Based on Hexagonal- WO_3
452 Nanowires for Multifunctional Applications, *Adv. Mater.* (2023) 2304420.
- 453 [32] K. Suematsu, M. Sasaki, N. Ma, M. Yuasa, K. Shimano, Antimony-Doped Tin Dioxide
454 Gas Sensors Exhibiting High Stability in the Sensitivity to Humidity Changes, *ACS Sens.*
455 1 (2016) 913-920.
- 456 [33] D. Feng, L. Du, X. Xing, C. Wang, J. Chen, Z. Zhu, Y. Tian, D. Yang, Highly Sensitive
457 and Selective NiO/WO_3 Composite Nanoparticles in Detecting H_2S Biomarker of
458 Halitosis, *ACS Sens.* 6 (2021) 733-741.
- 459 [34] B. Zhang, L. Wang, Y. Zhang, Y. Ding, Y. Bi, Ultrathin $FeOOH$ Nanolayers with
460 Abundant Oxygen Vacancies on $BiVO_4$ Photoanodes for Efficient Water Oxidation,
461 *Angew. Chem. Int. Ed.* 57 (2018) 2248-2252.
- 462 [35] B. Tong, Z. Deng, B. Xu, G. Meng, J. Shao, H. Liu, T. Dai, X. Shan, W. Dong, S. Wang,
463 S. Zhou, R. Tao, X. Fang, Oxygen Vacancy Defects Boosted High Performance p-Type
464 Delafossite $CuCrO_2$ Gas Sensors, *ACS Appl. Mater. Interfaces* 10 (2018) 34727-34734.

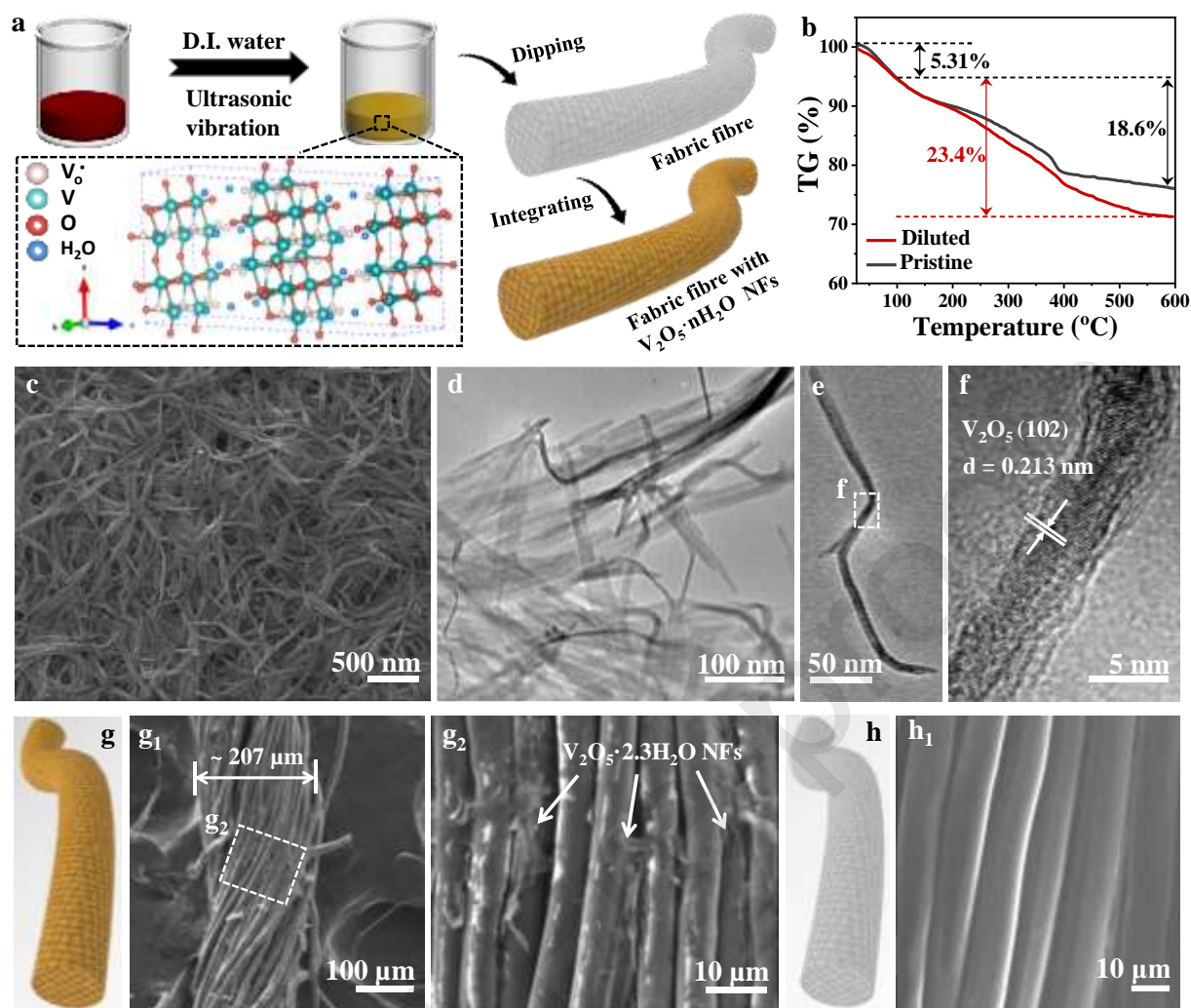


- 465 [36] K. Schneider, M. Lubecka, A. Czapla, V_2O_5 thin films for gas sensor applications, *Sens.*
466 *Actuator B Chem.* 236 (2016) 970-977.
- 467 [37] D. Yao, C. Dong, Q. Bing, Y. Liu, F. Qu, M. Yang, B. Liu, B. Yang, H. Zhang, Oxygen-
468 Defective Ultrathin $BiVO_4$ Nanosheets for Enhanced Gas Sensing, *ACS Appl. Mater.*
469 *Interfaces* 11 (2019) 23495-23502.
- 470 [38] X. Xing, L. Du, D. Feng, C. Wang, M. Yao, X. Huang, S. Zhang, D. Yang, Individual gas
471 sensor detecting dual exhaled biomarkers via a temperature modulated n/p
472 semiconducting transition, *J. Mater. Chem. A* 8 (2020) 26004-26012.
- 473 [39] L. Xu, C. Wang, X. Zhang, D. Guo, Q. Pan, G. Zhang, S. Wang, NO_x sensitivity of
474 conductometric $In(OH)_3$ sensors operated at room temperature and transition from p- to
475 n- type conduction, *Sens. Actuator B Chem.* 245 (2017) 533-540.
- 476 [40] H. Wu, J. Yu, G. Yao, Z. Li, W. Zou, X. Li, H. Zhu, Z. Huang, Z. Tang, Room temperature
477 NH_3 sensing properties and humidity influence of $Ti_3C_2T_x$ and $Ag-Ti_3C_2T_x$ in an oxygen-
478 free environment, *Sens. Actuator B Chem.* 369 (2022) 132195.
- 479 [41] D. Wang, D. Zhang, Y. Yang, Q. Mi, J. Zhang, L. Yu, Multifunctional
480 Latex/Polytetrafluoroethylene-Based Triboelectric Nanogenerator for Self-Powered
481 Organ-like MXene/Metal–Organic Framework-Derived CuO Nanohybrid Ammonia
482 Sensor, *ACS Nano* 15 (2021) 2911-2919.
- 483 [42] Y. Liu, H. Ji, Z. Yuan, H. Zhu, L. Kong, H. Gao, F. Meng, Hollow urchin $Co-Fe_2O_3$ with
484 outstanding selectivity and fast responding for ppb level NH_3 sensing via Lewis acid-base
485 effect, *Chem. Eng. J.* 474 (2023) 145620.
- 486 [43] K.-P. Yuan, L.-Y. Zhu, J.-H. Yang, C.-Z. Hang, J.-J. Tao, H.-P. Ma, A.-Q. Jiang, D.W.
487 Zhang, H.-L. Lu, Precise preparation of $WO_3@SnO_2$ core shell nanosheets for efficient
488 NH_3 gas sensing, *J. Colloid Interf. Sci.* 568 (2020) 81-88.
- 489 [44] F. Ranjbar, S. Hajati, M. Ghaedi, K. Dashtian, H. Naderi, J. Toth, Highly selective
490 MXene/ $V_2O_5/CuWO_4$ -based ultra-sensitive room temperature ammonia sensor, *J. Hazard.*
491 *Mater.* 416 (2021) 126196.
- 492 [45] D. Maity, R.T.R. Kumar, Polyaniline Anchored MWCNTs on Fabric for High
493 Performance Wearable Ammonia Sensor, *ACS Sens.* 3 (2018) 1822-1830.
- 494 [46] D. Lv, W. Shen, W. Chen, R. Tan, L. Xu, W. Song, PSS-PANI/PVDF composite based
495 flexible NH_3 sensors with sub-ppm detection at room temperature, *Sens. Actuator B*
496 *Chem.* 328 (2021) 129085.
- 497 [47] D. Zhang, Y. Yang, Z. Xu, D. Wang, C. Du, An eco-friendly gelatin based triboelectric
498 nanogenerator for a self-powered PANI nanorod/ $NiCo_2O_4$ nanosphere ammonia gas
499 sensor, *J. Mater. Chem. A* 10 (2022) 10935-10949.
- 500 [48] X. Wang, D. Zhang, H. Zhang, L. Gong, Y. Yang, W. Zhao, S. Yu, Y. Yin, D. Sun, In
501 situ polymerized polyaniline/MXene (V_2C) as building blocks of supercapacitor and
502 ammonia sensor self-powered by electromagnetic-triboelectric hybrid generator, *Nano*
503 *Energy* 88 (2021) 106242.
- 504 [49] Y. Fu, T. Wang, X. Wang, X. Li, Y. Zhao, F. Li, G. Zhao, X. Xu, Investigation of p-n

505 sensing transition and related highly sensitive NH_3 gas sensing behavior of SnPx/rGO
506 composites, Chem. Eng. J. 471 (2023) 144499.

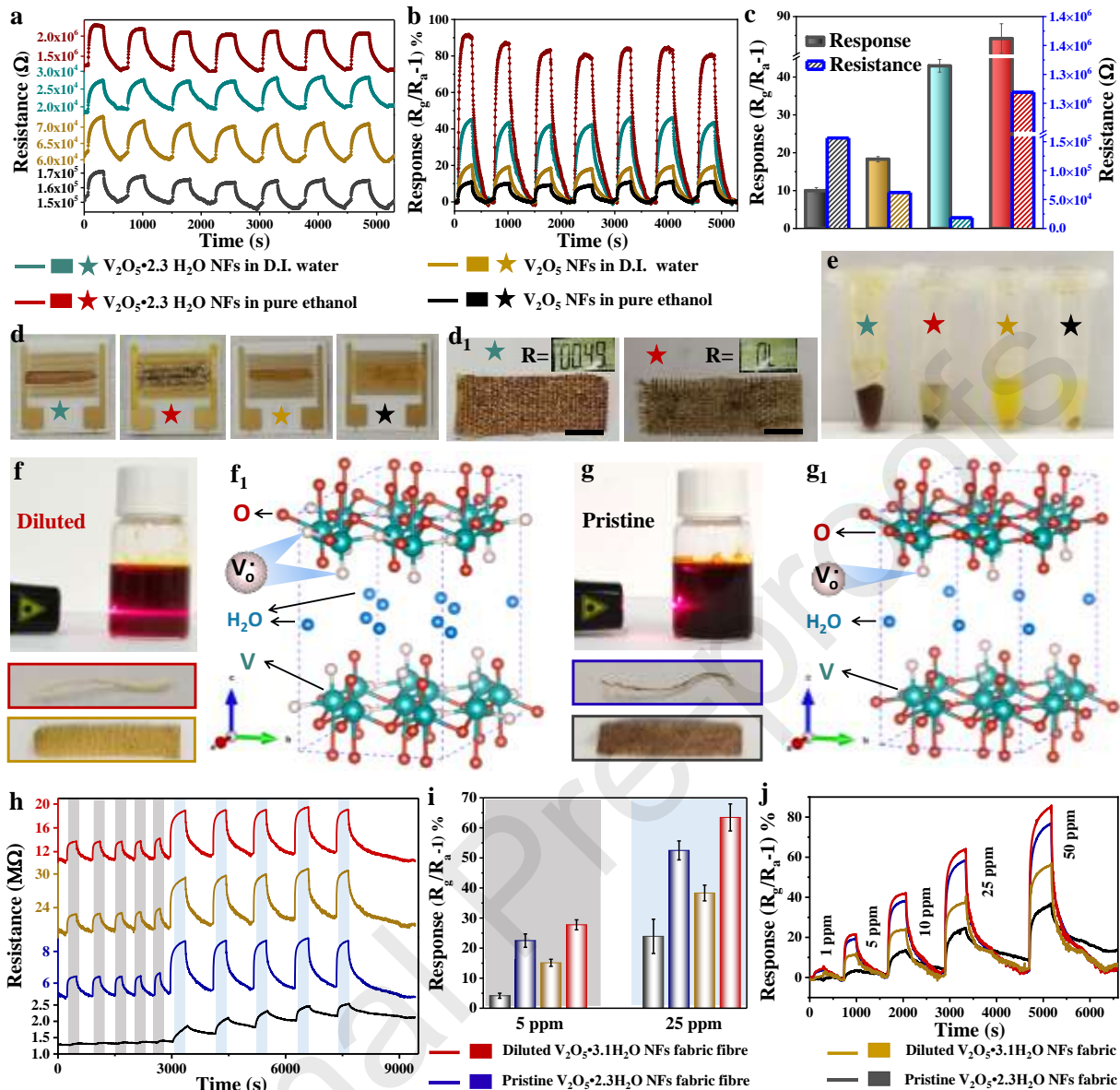
507

Journal Pre-proofs



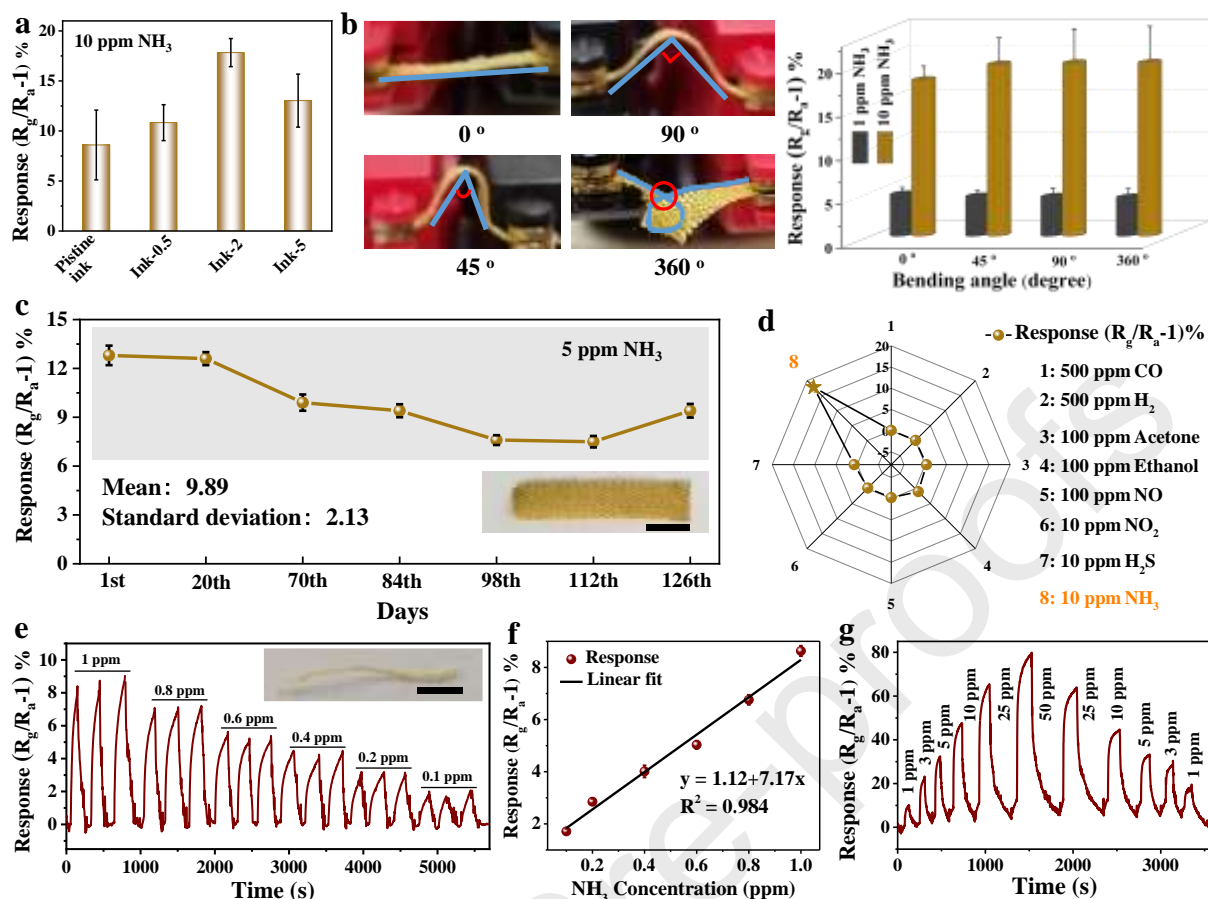
508

509 **Fig. 1.** The synthesis and characterization of $V_2O_5 \cdot nH_2O$ NFs. (a) The schematic diagram of
 510 diluting and integrating $V_2O_5 \cdot nH_2O$ NFs ink, and the simulated crystal structure of $V_2O_5 \cdot nH_2O$
 511 NFs. (b) The TGA curves of pristine and diluted $V_2O_5 \cdot nH_2O$ NFs. (c) The SEM, (d-e) TEM
 512 and (f) HRTEM images of pristine $V_2O_5 \cdot 2.3H_2O$ NFs. (g) The schematic diagram and (g_1 - g_2)
 513 SEM images of fabric fiber integrated with $V_2O_5 \cdot nH_2O$ NFs ink. (h) The schematic diagram
 514 and (h_1) the SEM image of bare fabric fiber.



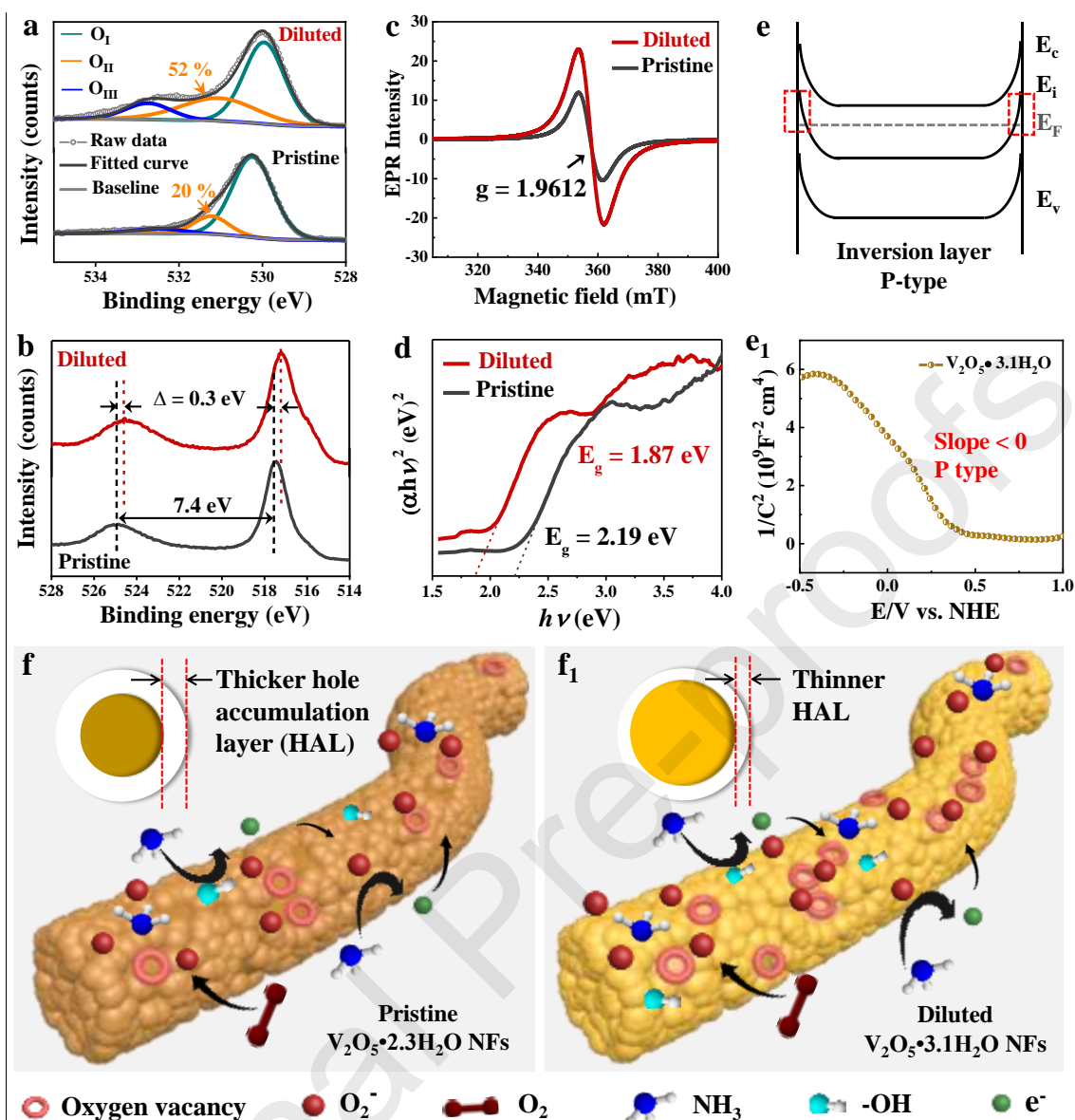
515

516 **Fig. 2.** The NH₃ sensing comparison between freeze-dried and annealed V₂O₅·2.3H₂O NFs
 517 powder being dispersed in D.I. water and pure ethanol, respectively. (a) The real-time resistance
 518 and (b) sensing curves to 10 ppm NH₃, and corresponding (c) histogram of baseline resistance
 519 and response value. (e) The photograph of above four dispersions and (d) integrated interdigital
 520 electrode. (d₁) The freeze-dried V₂O₅·2.3H₂O NFs dispersed in D.I. water and pure ethanol
 521 were integrated onto the fabric, respectively. The scale bars in (d₁) are 0.5 cm. The photographs
 522 and structures of (f-f₁) diluted and (g-g₁) pristine V₂O₅·nH₂O NFs inks. The “Tyndall effect”
 523 of diluted V₂O₅·3.1H₂O NFs ink irradiated by red light ($\lambda = 638$ nm). The comparison on NH₃
 524 sensing performance between diluted and pristine V₂O₅·nH₂O NFs inks integrated on fabric
 525 and the fabric fibre, respectively. (h) The real-time resistance curves and (i) the summarized
 526 responses. (j) The response curves to various NH₃ concentration. The RH of (a-b, h-j) is at ~
 527 22%.



528

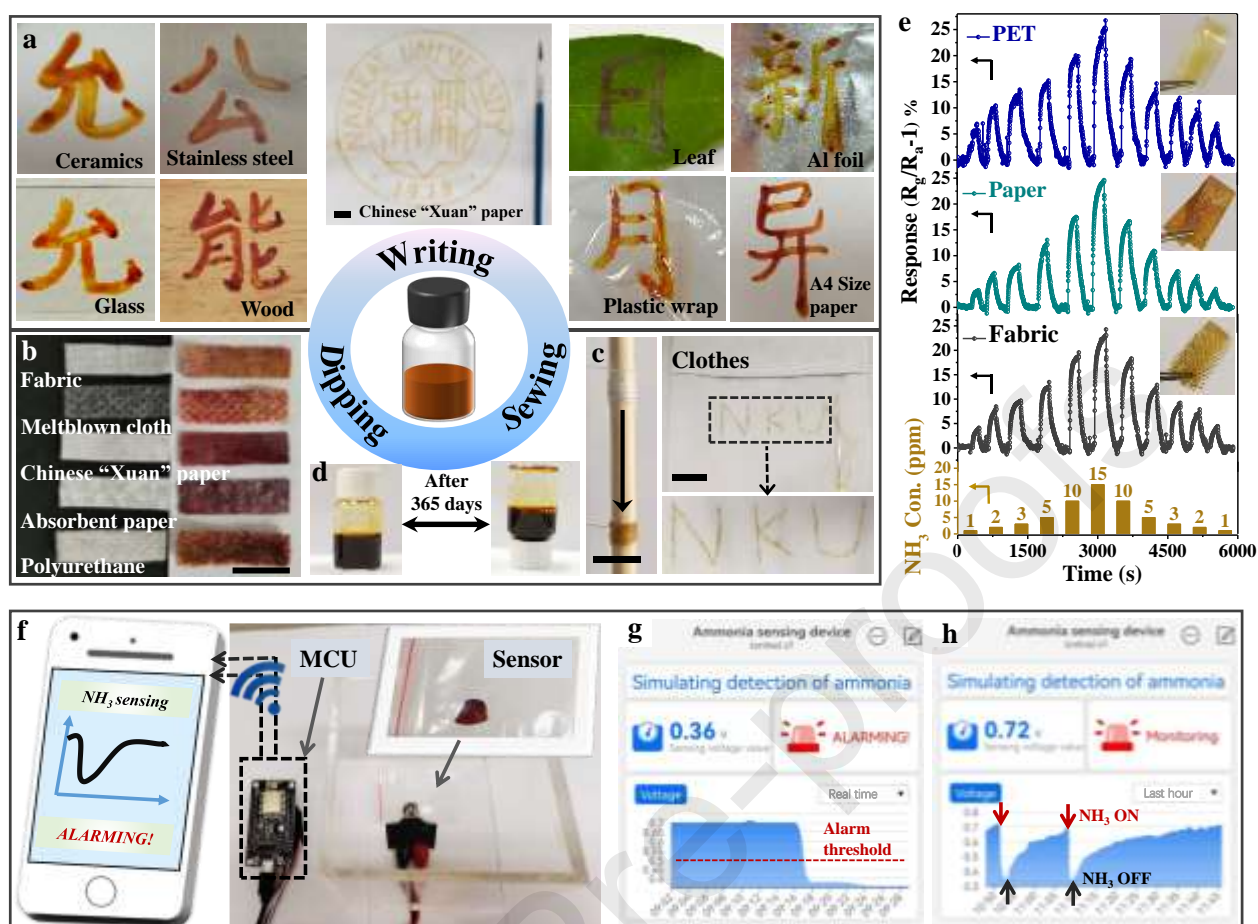
529 **Fig. 3.** The systematic NH₃ sensing evaluation of V₂O₅·nH₂O NFs ink integrated over fabrics:
 530 (a) The dilution-dependent sensing response of V₂O₅·nH₂O NFs ink, (b) the V₂O₅·3.1H₂O NFs
 531 fabric under various bending angle and their corresponding sensing responses, (c) the long-term
 532 stability and (d) selectivity of diluted V₂O₅·3.1H₂O NFs fabric. The NH₃ sensing evaluation of
 533 V₂O₅·3.1H₂O NFs fabric fiber: (e) The response curve to 0.1-1 ppm NH₃, (f) the relationship
 534 between sensing responses and NH₃ concentrations, (g) the response curve to various NH₃
 535 concentrations. The scale bars in (c) and (e) are 0.5 cm. The RH of (a-b, d, e-g) is at ~ 19% and
 536 RH of (c) is at ~ 19%-57%.



537

538 **Fig. 4.** The various characterizations on oxygen vacancy of pristine $V_2O_5 \cdot 2.3H_2O$ NFs and
 539 diluted $V_2O_5 \cdot 3.1H_2O$ NFs. High-resolution XPS spectra are related to (a) O 1s and (b) V 2p,
 540 (c) EPR spectra and (d) plots of $(\alpha h\nu)^2$ vs photon energy ($h\nu$). The schematic energy-band
 541 variation of $V_2O_5 \cdot nH_2O$ NFs. (e) An inversion layer marked with red rectangle and p-type
 542 surface conductivity. (e₁) The Mott-Schottky plot of $V_2O_5 \cdot 3.1H_2O$ NFs. The NH_3 sensing
 543 mechanism diagrams of (f) pristine $V_2O_5 \cdot 2.3H_2O$ NFs and (f₁) diluted $V_2O_5 \cdot 3.1H_2O$ NFs.

544



545

546 **Fig. 5.** The universal substrates-tolerant and multi means-integratable NH_3 sensing. (a) The
 547 $\text{V}_2\text{O}_5 \cdot 2.3\text{H}_2\text{O}$ NFs ink for drawing the school badge and the motto of Nankai University onto
 548 hard and flexible substrates. (b) The pristine $\text{V}_2\text{O}_5 \cdot 2.3\text{H}_2\text{O}$ ink was evenly integrated onto
 549 various flexible substrates as examples. (c) The diluted $\text{V}_2\text{O}_5 \cdot 3.1\text{H}_2\text{O}$ NFs ink integrated fabric
 550 fiber for sewing patterns into clothes. (d) The photographs of $\text{V}_2\text{O}_5 \cdot 3.1\text{H}_2\text{O}$ NFs ink after
 551 storing 365 days. (e) The NH_3 sensing of diluted $\text{V}_2\text{O}_5 \cdot 3.1\text{H}_2\text{O}$ NFs ink integrated on flexible
 552 substrates with PET, Chinese "Xuan" paper and fabric as examples, and "Con." in the ordinate
 553 represents concentration. The scale bars in (a, b, c) are all 1 cm. (f) Simulated detection of NH_3
 554 were conducted by intergrating the $\text{V}_2\text{O}_5 \cdot 3.1\text{H}_2\text{O}$ NFs ink onto sample bag and communicating
 555 with a smartphone. (g) Smartphone reading the real-time sensing parameters and the records of
 556 alarming to 10 ppm NH_3 and (h) the historical measurements. The RH of (e) is at $\sim 22\%$.

557 **Table 1.** Comparison of various NH₃ sensing materials in both presenting forms and NH₃
558 sensing.

Material type	Materials	Presenting forms	Substrates	Mechanical flexibility	Integrating means	W T ^{a)}	Response@Con. ^{c)}	T _{res} /T _{rec} time (s) @ Con. ^{c)}	LOD ^{b)} (ppm)	Refs. ^{b)}
	Co-Fe ₂ O ₃	powder	ceramic tube	No	spin-coating combined with calcination	275 °C	275% ^{d)} @10 ppm	7.2/5.4@10 ppm	0.01 ^{d)}	[42]
	MoO ₃ nanorods	powder	glass	No	spin-coating by mixing with solvent	200 °C	36% ^{d)} @5 ppm	230/267@5 ppm	~5 ^{d)}	[8]
	WO ₃ @SnO ₂ Core nanosheet shell	thin film	MEMS	No	dripping-coating by mixing with solvent	200 °C	1.5 ^{e)} @15 ppm	62/42@15 ppm	5 ^{d)}	[43]
SMOs based NH ₃ sensing materials	Ni-doped nanostructure	In ₂ O ₃ powder	ceramic tube	No	coating by mixing with solvent	140 °C	2732 ppm ^{e)} @50 ppm	23/10@50 ppm	~1 ^{d)}	[9]
	MXene/CuO composite.	solution	epoxy	Yes	spraying	RT	24.8 ^{d)} @100 ppm	43/26@100 ppm	~1 ^{d)}	[41]
	MXene/V ₂ O ₅ /CuWO ₄	precipitate	alumina sheet with interdigitated gold electrode	No	coating	RT	53.5 ^{d)} @51 ppm	1.6/4@51 ppm	1 ^{d)} 0.3 ^{d)}	[44]
	V ₂ O ₅ -nH ₂ O NFs	ink	ceramics, stainless steel, glass, wood, paper, leaf, Al foil, plastic wrap, fabric and polyurethane	Yes	dripping, writing, dipping and sewing	RT ^{b)}	~4.2% ppm ^{e)} @1 ppm	75/36@1 ppm	~0.1 ^{d)}	This work
Carbon based NH ₃ sensing	PANI/MWCNTs	-	polypropylene fabric	Yes	spray-coating and chemical polymerization	RT	61.54% ppm ^{e)} @20 ppm	9/30@20 ppm	0.2 ^{d)}	[45]

materials											
PEDOT:PSS nanowires	aqueous suspension	PET	Yes	spin-coating	RT	~2.2% ppm	^{g)} @6	96/318@6 ppm	0.1 ^{j)}	[19]	
PSS-PANI/PVDF	-	PVDF membrane	Yes	in-situ polymerization	RT	70% ^{g)} @1 ppm		160/400@1 ppm	~ 0.1 ⁱ⁾	[46]	
Pt-NDs/PPy-nanolayer@CNTs	powder	filter paper	Yes	coating by mixing with solvent	RT	~40% ^{g)} ppm	@50	2/~10@2 v/v%	~0.005 ^{j)}	[20]	
PANI/NiCo ₂ O ₄	powder	gelatin film	Yes	spin-coating	RT	4.67 ^{f)} @20 ppm		22/62@20 ppm	~ 0.5 ⁱ⁾	[47]	
PANI/MXene	solution	epoxy	Yes	dripping	RT	27% ^{g)} @5 ppm		27/5@5 ppm	~ 0.3 ⁱ⁾	[48]	
SnPx/rGO	powder	interdigitated electrodes	No	dripping	RT	117.5% ^{d)} to 40 ppm		126/306@10 ppm	0.0436 ^{j)}	[49]	

559 ^{a)} Working temperature, ^{b)} Room temperature, ^{c)} Concentration, ^{d)} Calculated by $(R_a/R_g - 1) * 100\%$, ^{e)} Calculated by R_a/R_g , ^{f)} Calculated by R_g/R_a , ^{g)} Calculated by $(R_g/R_a - 1) * 100\%$, ^{h)}
560 Limit of Detection, ⁱ⁾ Experimental measurements, ^{j)} Theoretical calculation, ^{k)} References.
561

562

563 **Declaration of interests**

564

565 The authors declare that they have no known competing financial interests or personal
566 relationships that could have appeared to influence the work reported in this paper.

567

568 The authors declare the following financial interests/personal relationships which may be
569 considered as potential competing interests:

570

571

572

573

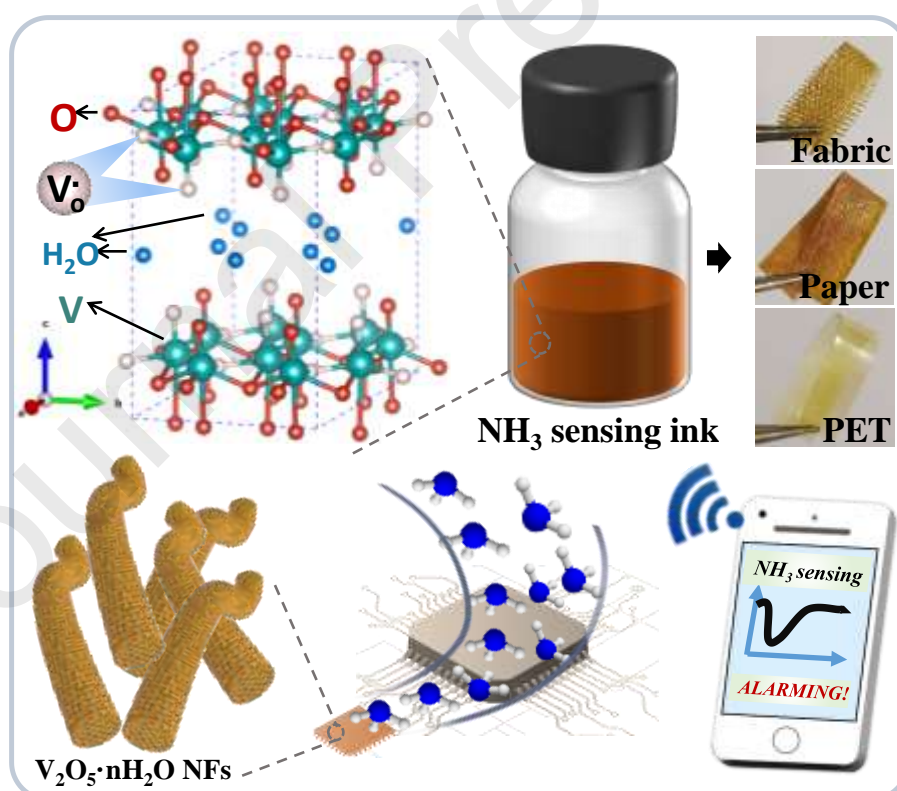
574

575

576

577

Graphical Abstracts



578

579

580

581

Highlights

1. The excellent dispersed and stable $\text{V}_2\text{O}_5 \cdot 3.1\text{H}_2\text{O}$ nanofibers ink has been developed.

- 582 2. The ink toward universal substrates-tolerant and multi means-integratable NH_3 sensing.
- 583 3. The oxygen vacancy governed NH_3 sensing mechanism is rationally interpreted.
- 584 4. Simulation on detecting NH_3 is conducted with reliable sensing response.
- 585

Journal Pre-proofs